Research Article/Araştırma Makalesi

Gazi AKADEMİK YAYINCILIK

GAZİ
JOURNAL OF ENGINEERING SCIENCES

Calculations of Structural Parameters and Optical Constants of Size Dependent ZrO_2

Gülsen Şahin[*a], Sultan Göktaş[b]

Submitted: 23.10.2023 Revised: 21.12.2024 Accepted: 01.03.2024 doi:10.30855/gmbd.0705N10

ABSTRACT

In this study, structural parameters and optical constants of size dependent zirconium dioxide (ZrO_2) nanostructures were calculated. The effect of particle size was investigated on the calculated structural and optical parameters/constants. ZrO_2 nanostructures were produced by chemical route. To change the grain size of the ZrO_2 nanostructures, different annealing temperatures (450-550 °C) were applied. The x-ray diffraction (XRD), scanning electron microscope (SEM), and ultraviolet/visible region (UV-Vis) spectroscopy measurement results were used to calculate the structural and optical parameters/constants. The results of XRD measurement showed the ZrO_2 nanostructures were crystallized in single tetragonal (cubic) ZrO_2 phase. SEM results exhibited dense and homogeneous surfaces and enhanced surface grains with increased annealing temperature. The compositional formation of ZrO_2 nanostructures were proved by electron dissipated x-ray and mapping analysis. Optical measurements were strongly changed dependent on the grain size (G_S). The calculated structural parameters such as crystallite size, lattice parameter (a), microstrain, and dislocation density were showed that the powerful variation according to the G_S. The computed optical constants such as refractive index, extinction coefficient, reel and imaginer dielectric constants of the ZrO_2 samples were highly varied upon the G_S. The variant in these calculated parameters/constant were extremely promising for the optic and dielectric applications.

Keywords: ZrO_2, Optical constant, Extinction coefficient, Refractive index, Reel dielectric constant

[a,*] Adıyaman University, Faculty of Education, Department of Science
02040 - Adıyaman, Türkiye
Orcid: 0000-0003-4891-041X
e mail: gsahin@adiyaman.edu.tr

[b] Harran University, Faculty of Science and Arts, Department of Chemistry
63290 - Şanlıurfa, Türkiye
Orcid: 0009-0000-7084-9710

*Corresponding author:
gsahin@adiyaman.edu.tr

Büyüklüğe Bağlı ZrO_2 Nanoyapılarının Yapısal Parametreleri ve Optiksel Sabitlerinin Hesaplanması

ÖZ

Bu çalışmada boyuta bağlı zirkonyum dioksit (ZrO_2) nanoyapılarının yapısal parametreleri ve optik sabitleri hesaplanmıştır. Parçacık boyutunun, hesaplanan yapısal ve optik parametreler/sabitler üzerindeki etkisi araştırıldı. ZrO_2 nanoyapıları kimyasal yolla üretildi. ZrO_2 nanoyapılarının tane boyutunu değiştirmek için farklı tavlama sıcaklıkları (450-550°C) uygulandı. Yapısal ve optik parametreleri/sabitleri hesaplamak için x-ışını kırınımı (XRD), taramalı elektron mikroskobu (SEM) ve ultraviyole/görünür bölge (UV-Vis) spektroskopisi ölçüm sonuçları kullanıldı. XRD ölçümü sonuçları, ZrO_2 nanoyapılarının tek tetragonal (kübik) ZrO_2 fazında kristalleştiğini gösterdi. SEM sonuçları, yoğun ve homojen yüzeyler ve artan tavlama sıcaklığıyla sayısı artan yüzey taneleri sergiledi. ZrO_2 nanoyapılarının bileşiksel oluşumu elektron dağılımlı x-ışını ve haritalama analizi ile kanıtlanmıştır. Optik ölçümler tane boyutuna (G_S) göre büyük ölçüde değişti. Kristal boyutu, örgü parametresi (a), mikro-gerilim ve dislokasyon yoğunluğu gibi hesaplanan yapısal parametreler, G_S'ye bağlı olarak ciddi bir değişim gösterdi. ZrO_2 numunelerinin kırılma indisi, sönüm katsayısı, reel ve sanal dielektrik sabitleri gibi hesaplanan optik sabitleri G_S'ye bağımlı olarak ciddi oranda değişti. Hesaplanan bu parametrelerdeki/sabitlerdeki değişkenlik, optik ve dielektrik uygulamalar için son derece umut vericidir.

Anahtar Kelimeler: ZrO_2, Optiksel sabit, Yok olma katsayısı, Kırılma indisi, Reel dielektrik katsayısı

To cite this article: G. Sahin and S. Goktas "Calculation of Structural Paramaters and Optical Constants of Size Dependent ZrO2," *Gazi Journal of Engineering Sciences*, vol.10, no.1, pp. 114-124, 2024. doi:10.30855/gmbd.0705N10

1. Introduction

In many practical applications, it is possible to make life easier by using nanostructured thin films. They can be preferred for making reflective or antireflective filters, circuit candidates, memory disks, memory disc, biological ceramics, sensors, and lasers [1-5]. In this context, attractive physical characteristics of Zirconia (ZrO_2) thin film such as having a high dielectric constant, a relatively higher melting point (2680°C), high chemical stability and wide band gap (4.7eV-7.8eV), make it extraordinary metal oxide semiconductors [6]. In addition to, its high thermal stability, high refractive index, and low thermal conductivity capacities lead to be commercially used as dielectric and insulator in various microelectronic applications viz. dynamic random-access memory, radio frequency, analog/mixed signal (RF/AMS) integrated circuits, and non-volatile resistive random-access memory [3,5].

It was reported that ZrO_2 could have different crystal-like phases such as monoclinic, tetragonal, and cubic dependent on high temperature reflecting polymorphic structure [7,8]. However, this high temperature phases can be maintained at room temperature using suitable oxide dopants [9-11]. Even for the pure ZrO_2 thin films it can be achieved owing to low crystallite size and compressive stress [12]. But the undoped ZrO_2 has deteriorated by some consequential issues. The small crystallization due to low temperature processing resulted in the enhanced additional leakage currents through the crystal boundaries and creating highly thick intersectional sheets [13]. In addition to, producing high dielectric constant (κ) metal oxide nanostructured thin films utilizing chemical solution-based method needs a relatively high sintering temperature of over 450 °C due to high pyrolysis and desiccation temperature of prototypical forerunners [14]. Annealing at relatively high temperatures is an effectual way to remove the defects (like oxygen vacancies) and impurities (like secondary phases) from metal-based oxide nanomaterials resulting into tolerable discharge and electrical capacity as well as high crystallization [15,16].

Recently, several fabrication of nanostructured thin films have been followed to product zirconia-based high-κ gate dielectric viz. sol-gel dip/spin coating, atomic layer deposition, spray pyrolysis, chemical vapor deposition, reactive RF sputtering, and electron beam evaporation [13,17]. Amongest all the solution-based sol-gel technique is currently becoming the most popular route owing to its clarity, economic, low treating temperature, practical use, and pile of yield. Some concern study has been outlined about the size dependent characteristics of sol-gel derived ZrO_2 thin films. However, a detailed work on the structural and optical properties, structural parameters, and linear optical constants of the ZrO_2 is rare. Therefore, in the present study the grain size dependent structural and optical characteristics, structural parameters and optical constants have been investigated.

2. Experiment and Calculation Techniques

To prepare ZrO_2 solution, zirconyl chloride octahydrate ($ZrOCl_2 \cdot 8H_2O$) was used for the parent solution. The molar ratio (0.01M) of chemical powder was utilized as Zr^{+2} source and it was dissolved by mixed solution of methanol (96,15 at. %) and glacial acetic acid (3,85 at .%). The desired ZrO_2 solution was get ready via vigorously mixing on the magnetic stirrer for 30-60 minutes at 50 °C. The final solution bath was aged by stirring at room conditions for 24 hours to have gel solution, which is essential for highly uniform film structure. Before coating, the glass facets were rinsed with deionized water. It was then ultrasonically cleaned in an ethanol and acetone ultrasonic bath for 5 minutes. In cleaning process, the glass surfaces were finally placed in the plasma cleaner to remove waste organic hanging bonds and precision cleaning. The cleaned glass substrates were immersed in the resulting solution and covered in air at 350°C. Films grown on the glass surfaces by sol-gel dip coating method and they were annealed at 450 °C, 500 °C and 550°C for 60 minutes in an air atmosphere to get desired grain size (G_S).

The latest emerging ZrO_2 thin films were constructionaly characterized via X-ray diffraction (XRD) with a Rigaku Ultima III diffractometer though employing CuK_α radiation (λ =0.15406 nm) at 30 mA and 40 keV from 20 to 70°. To calculate the average crystallite size (D_{hkl}), [13] the Debye Sherrer's equation as following as:

$$D_{hkl}=0.9\lambda/\beta.cos\theta \quad (1)$$

where λ is the wavelength of X-rays used, θ is the angle of diffraction and is the full width at half maximum. Similarly the other structural parameters like dislocation density (δ) and micro strain (ε) were computed according to the followed formulas:

$$\delta = 1/(D_{hkl})^2 \quad (2)$$

$$\varepsilon = \beta/4\tan\theta \quad (3)$$

The lattice parameters, a and c of the tetragonal ZrO_2 can be obtained according to the equations given below:

$$a_t=d_{h00}\ h;\ c_t=d_{h0l}\ (h^2+l^2)^{1/2} \quad (4)$$

In this equation the d_{hkl} ($d_{hkl}=a_t/((h^2+k^2+l^2)/(c_t/a_t))^{1/2}$) represents interplanar distance for the tetragonal lattice and (hkl) shows Miller indices. The morphology, surface, grain size, and atomic analysis and mapping were recognized using a scanning electron microscope (SEM) equipped by an energy dispersive X-ray (EDX) tool.

To research the optical characteristics like transmittance and absorbance, the UV–Vis (PerkinElmer 45) spectra was performed. The corresponding transmittance, absorbance and reflectance were than represented and the band gap energy (E_g), refractive index (n), extinction coefficient (k), and reel/imaginer dielectric constants were computed. To calculate E_g and k as well as other related parameters of the nanostructures Beer-Lambert law [17] was used as following:

$$I=I_0e^{-\alpha d} \quad (5)$$

where I is the intensity of the transmitted light, I_0 is the intensity of the incident light, d shows the thickness of the nanostructured layer, and α is the linear absorption coefficient of the materials. In equation (5) α can be calculated as [18]:

$$\alpha = (1/d)\ ln\ (1/T) \quad (6)$$

in that T is the transmittance. The connection between the α and the photon energy ($h\upsilon$) is given as follows [19]:

$$(\alpha h\upsilon)^2 = A(h\upsilon - E_g)^m \quad (7)$$

where A and m are constant coefficients. For indirect transitions, m=2 and for direct transitions n=1/2. Moreover, k and n can be obtained by using reflectance (R) and α as given in equation of (8) and (9) as below [20]:

$$k\ (\lambda)=\alpha\lambda/4\pi \quad (8)$$

$$n(\lambda)= ((1+R(\lambda))/(1-R(\lambda)))+((4R(\lambda))/(1+R(\lambda)-k^2(\lambda))^{1/2} \quad (9)$$

where λ represents of the acted photon wavelength. Finally, the corresponding reel and imaginary dielectric

constants $\mathcal{E}_r$ and $\mathcal{E}_i$ are calculated via using the followed equations [19]:

$$\mathcal{E}_r(\lambda)=n(\lambda)^2-k(\lambda)^2 \quad (10)$$

$$\mathcal{E}_i(\lambda)=2n(\lambda)k(\lambda) \quad (11)$$

3. Results and Discussions

3.1. Calculation of structural parameters by using XRD analysis

The XRD analysis was used to investigate the crystal structure and phase composition of the deposited nanostructures. The XRD patterns of the ZrO_2 nanostructures sintered at 450 °C, 500 °C, and 550°C were given in Fig.1. All nanostructured films show the tetragonal phase with highly oriented (101) Miller crystal plane and polycrystalline nature. The observed other (110), (112), and (211) Miller crystal planes are also indexed for the tetragonal phase. XRD patterns also show there are no metallic or secondary phases in the host ZrO_2 lattice system. The results agree with the research on ZrO_2 thin film [18]. According to Fig. 1, the ZrO_2 nanostructures represent the best crystallization at 550 °C. The average crystallite size (D_{hkl}) [13] calculated using the Debye Sherrer's equation (1) was given in Table 1. The mean D_{hkl} for thin film samples turned out to be 21 nm.

Table 1. The full-width half-maximum, diffraction angle, crystallite size, dislocation density, micro-strain, and lattice parameter of the prepared ZrO_2 nanostructures having various grain sizes

Annealing temperature (°C)	FWHM (β_o)	2θ(deg.)	D_{hkl}(nm)	δx10^{-3}	Ɛx10^{-3}	a;c (Å)
Z3-450	0.80	30.42	10	10.0	12.8	0.5106;5.076
Z3-500	0.53	30.50	15	4.44	8.48	0.5092;5.063
Z3-550	0.38	30.52	21	2.26	6.08	0.5089;5.060

To obtain better crystalline quality, namely increased crystallite size, by providing crystallization in ZrO_2 thin film samples, annealing was done at different temperatures. Figure 1 shows the XRD patterns of ZrO_2 thin film samples annealed at different temperatures. Among all samples, the ZrO_2 nanostructure sintered at 550 °C has the best crystalline quality.

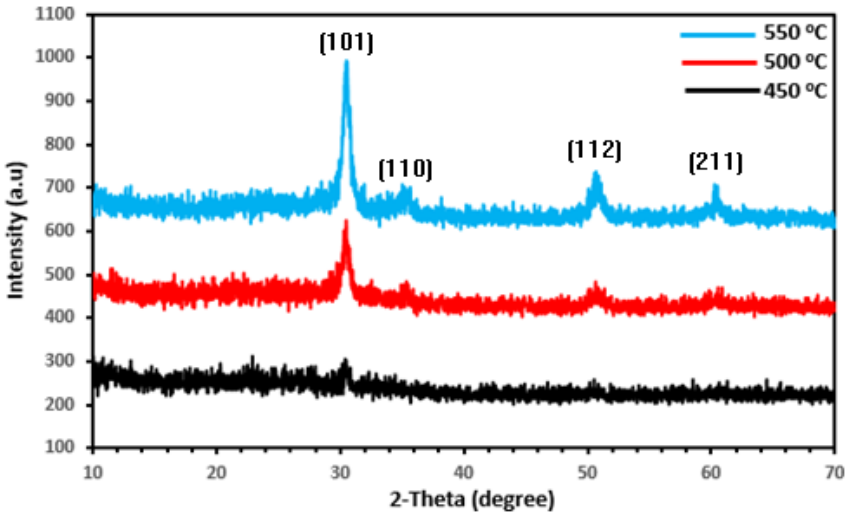

Figure 1. XRD patterns of the deposited ZrO_2 nanostructures with different grain sizes

The calculated D_{hkl} increases with increasing annealing temperature (Table 1). Considering the analysis of nanostructured ZrO_2 thin films prepared at different operating temperatures by Deshmukh and Bari's spray pyrolysis technique; they found that the structure of the film was completely crystallized with an increase in annealing temperature. Additionally, grain growth increased in mobility with increasing temperature. Again, when the literature on the effect of annealing temperature was scanned, it was seen that; Hadi et al., annealed and analyzed the Li doped (ZrO_2) nanostructures produced using the spray pyrolysis (CSP) method at 300^{O}C, 400^{O}C, and 500^{O}C. As a result, they observed that the grain size values, average roughness increased with increasing in sintering temperature. The lattice parameters, *a and c* of the ZrO_2 nanostructures calculated (by using formula 4) for different annealing temperatures (for 450 ºC -550ºC) were obtained as in Table 1. It was observed that the *a* and *c* values decreased as the $D_{(hkl)}$ increased. Different ionic sizes in lattice defects, perfect arrangement of atoms, impurity formations can cause differences in *a* and *c* values (see Table 1) dislocation density, (see equation 2), and micro strain (formula 3) as obtained. Different values of δ and Ɛ in Table 1 confirm the variation in lattice parameters. The difference in the lattice parameters, *a* and *c* may also be due to the lattice mismatch between the ZrO_2 nanostructures and the glass sample holder [21-24].

3.2. Estimation of average grain size from SEM analysis

SEM images and EDX/mapping analysis of ZrO_2 nanostructures produced at different annealing temperatures were shown in Figs. 2a-d. The film surfaces have smooth and dense morphology. The grain sizes changes about 20-200 nm, 30-250 nm, and 20-300 nm were estimated for the ZrO_2 nanostructures sintered at temperature range of 450 ºC, 500 ºC, and 550 ºC, respectively. This result is highly agreement with the XRD analysis. Spherical-like grains were observed for the ZrO_2 nanostructures annealed at different temperatures of 450 ºC, 500 ºC and 550 ºC. As a result of thermal energy leading simple displacement of atoms and anisotropic aggregation of crystallites/grains; As seen in Figure 2, annealing temperature affects G_S. The particle or G_S of the nanostructured films increases due to annealing process. Méndez-López et al. [20] prepared ZrO_2 nanostructures by sol-gel dip coating method and investigated the effect of annealing temperature on the structural and optical properties of the ZrO_2 nanostructures. The SEM facet patterns of their nanostructures annealed at 450ºC, and 550ºC showed the increased G_S of ZrO_2 nanostructures with increasing sintering temperature (Figs. 2a-c). AISI 316L stainless steel was coated with nanostructured zirconia using the sucrose-supported sol-gel dip coating method by Mishra et al. [15]. As a result of SEM analysis, it was seen that the particle sizes of zirconia thin films increased dependent on enhanced sintering temperature, raised from 300 ºC to 650 ºC. The presence of the Zr and O was observed from the EDX and mapping analysis (red and green colors represent the Zr and O atom, respectively) as seen in Fig. 2d.

3.3. Calculation of optical parameters and constants

3.3.1. Determination of optical band gap and reflectance

Optical transmittance and absorbance spectrum of the prepared nanostructured ZrO_2 film samples were exhibited in Figs. 3a and b for the wavelength range of 200-900 nm. As seen in Fig.3a, the transmittance suddenly reduces as the particle size increases. On the other hand, the opposite trend has been observed as expected for the absorbance of the nanostructured ZrO_2 films. The sharp reduction in certain wavelengths and oscillations in Uv-Vis spectrums show homogeneity and quality
of the fabricated films [15, 22].

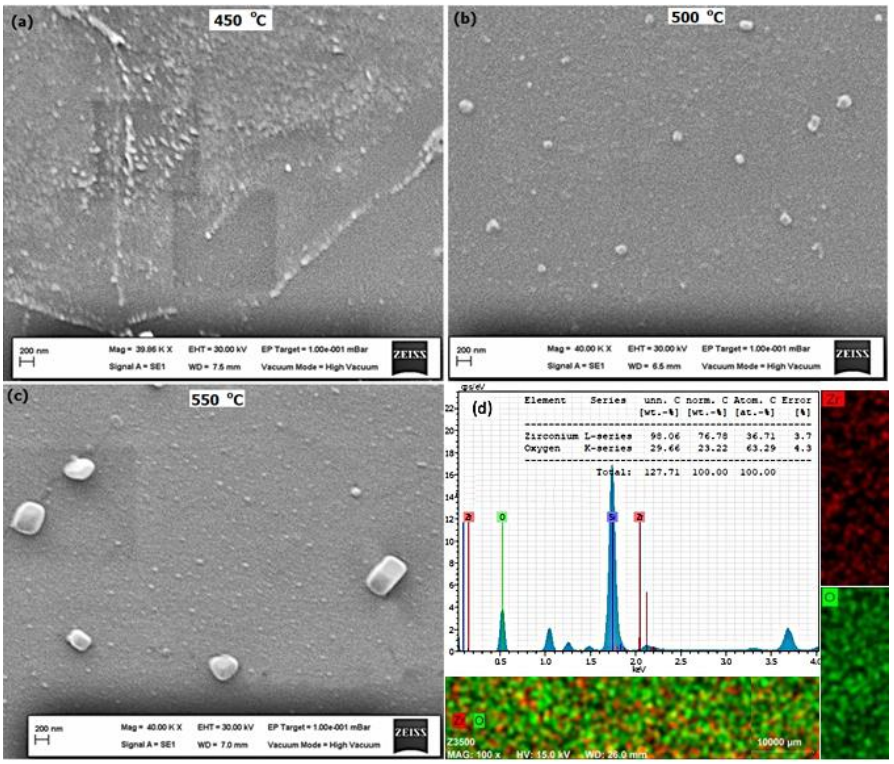

Figure 2. SEM surface images (a-c) and EDX/mapping analysis (d) of the deposited ZrO_2 nanostructures with different grain sizes

The band gap energy (E_g) of the nanostructures is found by extrapolation of the linear part of the curve between $(ah\nu)^2$ and $h\nu$ as given in Fig.3c (using equations 5, 6, and 7), indicating increment of the E_g from 3.96 to 4.24 eV with increase in grain size, accomplished by sintering process. This may be due to the increased crystallite/grain size or variation in lattice parameters of the film samples as well as the presence of the defects within the ZrO_2 lattice system [17,13].

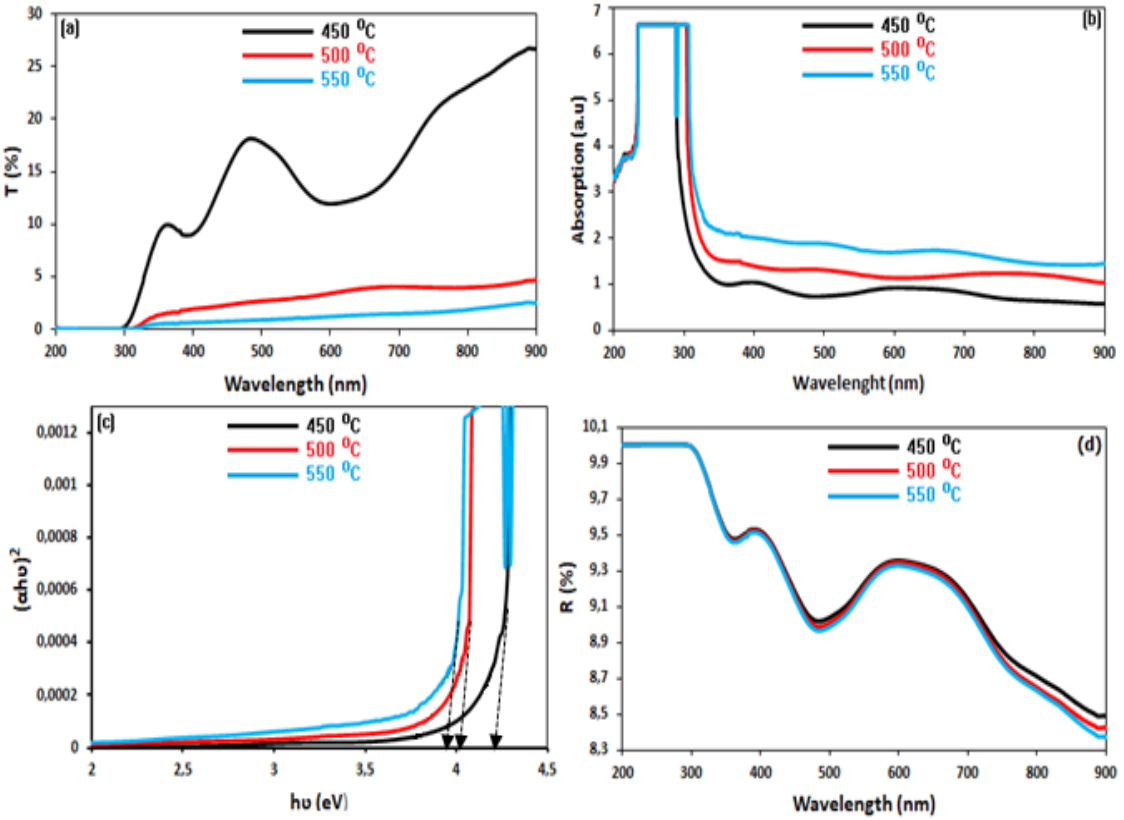

Figure 3. Transmittance (a), absorbance (b), variation of $(\alpha h\upsilon)^2$ dependent on $h\upsilon$ (c), and reflectance (d) plots of the deposited ZrO_2 nanostructures with different grain sizes

To calculate the optical constants of the presented ZrO_2 films, the reflectance has been obtained by using the relationship between the ($R=(1-T)^{1/2}*e^{\alpha}$) reflectance, absorption, and transmittance. Fig. 3d shows the plot of R upon on wavelength and annealing temperature (T_A). It shows decrement via enhanced particle size and T_A. This reduction and low values of R are mainly due to the poor transmission and relatively high absorbance as seen in Fig. 3a and b. The observations are in good agreement with previously reported studies on ZrO_2 nanostructures [13] and [15-24].

3.3.2. Determination of optical constants

It can be said that the n is one of the most main optical parameter, highly related to the electronic polarizability of ions and the internal field inside substances. On the other hand, the other important optical parameter k is closely associated to the absorbance of the matter. Their variations with the λ (200–900 nm) were presented Fig. 4 (a-b) for various grain size as determined above. The k of the film samples exhibits an enhancement with improved $D_{(hkl)}$ or G_S. These behaviors can be attributed to the α and hence absorbance as seen in Fig. 3b. Amongst all, the highest k values were observed for the ZrO_2 nanostructures having grain sizes within the range of 20-300 nm. On the contrary, the n values show opposite trend with k values, whereas it exhibits the same behavior with reflectivity. It is obvious that the n values of the ZrO_2 nanostructures decrease with increasing $D_{(hkl)}$ or G_S. Increasing or decreasing n is probably related to the compositional modifications due to the different grain sizes, which result in decrease/increase of the optical quality of the ZrO_2 nanostructures. These findings are in accordance with refs. [25] and [26].

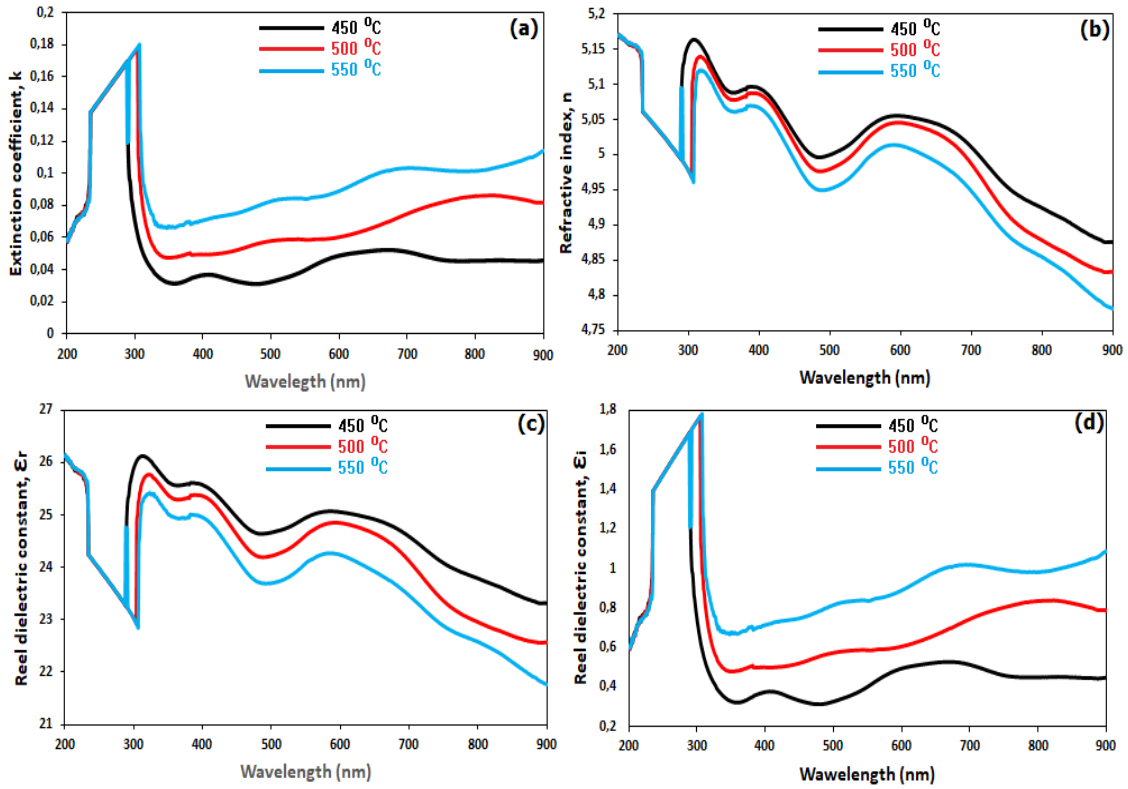

Figure 4. Wavelength depended on the extinction coefficient (a), refractive index (b), reel (c) and imaginary(d) dielectric constants of the deposited ZrO2 nanostructures with different grain sizes

It is possible to obtain reel and imaginary dielectric constants of the matter by using equations of 10 and 11 for the zirconia nanostructures. Both form the dielectric constant of the matter, representing the linear reaction of the order to action electromagnetic radiations i.e. interplay between the electrons of the structure with photons. The plots of both were given in Fig. 4c-d, with respect to the G_S and λ. As seen in these Figs., the $\mathcal{E}_r(\lambda)$values decrease, whereas the $\mathcal{E}_i(\lambda)$ values increase with increasing G_S. It is also seen that the $\mathcal{E}_r(\lambda)$values decrease by wavelength at visible region while the $\mathcal{E}_i(\lambda)$ values increase. In addition to, the trend of $\mathcal{E}_r(\lambda)$values is nearly same with the n, whereas the $\mathcal{E}_i(\lambda)$ values show the same trend with k. Moreover, $\mathcal{E}_r(\lambda)$values are higher than those of the $\mathcal{E}_i(\lambda)$ values because of their corresponding n and k values. These results can be attributed to the change in G_S carried out by sintering temperature, which leads to increase in polarizability of the system due to variant in charge imbalance, especially in the nanocrystalline structures. The observed outcomes are in good agreement with the study on ZrO_2 or oxide-based nanostructures having various G_S carried out by thickness or sintering temperatures [27,28].

Table 2. A comparison of the certain structural and optical parameters/constants of the sol-gel grown ZrO_2 thin films with the previously synthesized ZrO_2 thin films, produced by sol-gel method

GS/D_{hkl}(nm)	δx10^{-3}	ε x 10^{-3}	Eg(eV)	n (at visible range)	k (at visible range)	εr (at visible range)	Ref
(20-200)/10	10.0	30.42	3.96	5.02-5.10	0.039-0.041	24.6-25.7	This study
(30-250)/15	4.44	30.50	4.05	4.98-5.08	0.05-0.063	24.2-25.4	This study
(20-300)/21	2.26	30.52	4.24	4.95-5.07	0.071-0.098	23.4-24.9	This study
(----)/3-9.9	----	----	----	1.60-2.40	-----	-----	[31]
(----)/10.3	----	----	5.72	2.1	-----	-----	[18]
(----)/15.6	----	----	5.10	-----	-----	-----	[32]
(5-12)/---	----	----	----	-----	-----	-----	[23]

Table 2 summarizes some recent studies on ZrO_2 thin films derived by sol-gel technique. The presented characteristics and parameters are relatively superior to the previously reported studies on the ZrO_2 thin films. The observed relatively low E_g values and higher n values reflects the influences of different grain/crystallite

and used chemical precursors as well as experimental conditions. The presented study is also one of the best examples of the structural and optical properties and parameters/constant of the sol-gel derived ZrO_2 thin films at wide range of grain/crystallite size among all the considered ZrO_2 thin films, whose optical constant have not been studied in more detail yet, as given in table 2. In addition, this table also reflects the importance of the presented study accordingly [29,30].

4. Conclusions

In this study, the influences of the grain size (G_S) on the calculated structural and optical parameters and constants of the zirconia dioxide (ZrO_2) nanostructures have been investigated for the first time. The ZrO_2 nanostructures crystallized within a tetragonal phase and preferred direction onwards (111) Miller plane. Crystallite size (D_{hkl}) and orientation degree of ZrO_2 have significantly affected by G_S. As the G_S values rise the calculated structural parameters D_{hkl} increases while computed micro-strain, dislocation density, and lattice parameter values decrease. The increasing of the G_S has proved by SEM analysis, including EDX and mapping investigations, showing the existence of Zr and O elements. Uv-Vis spectrophotometer investigations show decreased absorbance while reflectance and transmittance increase with increasing G_S. The calculated band gap values increase from 3.85 to 4.05 eV by enhance of G_S. With enhanced G_S the opposite trend has been observed in the refractive index and the extinction coefficient values. Amongst all the highest refractive index values have been detected for the lowest G_S distribution, whereas the lowest extinction coefficient values have been determined. Like the refractive index values, the reel dielectric constant values of the ZrO_2 have also shown the same behavior, while the imaginer dielectric constant values show the same trend with the extinction coefficient values. The observed variants are possibly because of the disparity in crystallite/grain size, nanostructure, polarizability, and packing density of the ZrO_2 nanostructures. These findings are in good agreement with those issued on ZrO_2 nanostructures produced by various methods. In addition to, this research is the first record of the effects of G_S on the computed structural and optical parameters and constants of ZrO_2 synthesized by sol–gel dip-coating technique, relatively the most practical and economical process to fabricate nanostructured materials used for the number of demands in the next dielectric and optic applications.

Acknowledgments

The authors are grateful to thin film research group led by Prof. Dr. Abdullah GÖKTAŞ, Department of Physics, Faculty of Arts and Science to guide the authors during this scientific research at Harran University/TURKEY.

Conflict of Interest Statement

The authors declare that there is no conflict of interest.

References

[1] A. V. Rudakova, Alexei V. Emeline, Kirill M. Bulanin, Lyudmila V. Chistyakova, Maria V. Maevskaya and Detlef W. Bahnemann, "Self-cleaning properties of zirconium dioxide thin films," *Journal of Photochemistry & Photobiology A: Chemistry*, vol. 367, pp. 397–405, 2018. doi:10.1016/j.jphotochem.2018.08.037

[2] S. Goktas, A. Tumbul and A. Goktas, "Growth Technique–Induced Highly C-Axis-Oriented ZnO: Mn, ZnO: Fe and ZnO: Co Thin Films: A Comparison of Nanostructure, Surface Morphology, Optical Band Gap, and Room Temperature Ferromagnetism," *Journal of Superconductivity and Novel Magnetism*, vol. 36, pp. 1875–1892, 2023. doi:10.1007/s10948-023-06630-4

[3] S. Park, J.M. Vohs and R.J. Gorte, "Direct oxidation of hydrocarbons in a solid-oxide fuel cell," *Nature*, vol. 404, no. 6775, pp. 265-267, 2000. doi:10.1038/35005040

[4] S. Sultana, M.Z. Khan, K. Umar and M. Muneer, "Electrical, thermal, photocatalytic and antibacterial studies of metallic oxide nanocomposite doped polyaniline," *Journal of Materials Science & Technology*, vol. 29, no. 9, pp. 795–800, 2013. doi:10.1016/j.jmst.2013.06.001

[5] C-Y. Lin, C-Y. Wu, C-Y. Wu, T-C. Lee, F-L. Yang, C. Hu and T-Y. Tseng, "Effect of top electrode material on resistive switching properties of ZrO2 film memory devices," *IEEE Electron Device Letters*, vol. 28, no. 5, pp. 366–368, 2007. doi:10.1109/LED.2007.894652

[6] B. Coskun, T. Asar, U. Akgul, K. Yildiz and Y. Atici, "Investigation of structural and electrical properties of Zirconium dioxide thin films deposited by reactive RF sputtering technique," *Ferroelectrics*, vol. 502, no. 1, pp. 147-158, 2016. doi:10.1080/00150193.2016.1235453

[7] M. T. Soo, G. Kawamura, H. Muto, A. Matsuda, Z. Lockman and K. Y. Cheong, "Design of hierarchically meso–macroporous tetragonal ZrO2 thin films with tunable thickness by spin-coating via sol–gel template route," *Microporous and Mesoporous Materials*, vol. 167, pp. 198–206, 2013. doi:10.1016/j.micromeso.2012.09.010

[8] L. Liu, C. Li, Y. Chen, X. Zhang, L. Li and Y. Wang, "Phase transformation of ZrO2 nanocrystals induced by Li+," *Materials Letters*, vol. 79, pp. 75–77, 2012. doi:10.1016/j.matlet.2012.03.112

[9] S. Tekeli and U. Demir, "Colloidal processing, sintering and static grain growth behavior of alumina-doped cubic zirconia," *Ceramics International*, vol. 31, no. 7, pp. 973-980, 2005. doi:10.1016/j.ceramint.2004.10.011

[10] S.K. Durrani, J. Akhtar, M. Ahmad and M.A. Hussain, "Synthesis and characterization of low density calcia stabilized zirconia ceramic for high temperature furnace application," *Materials Chemistry and Physics*, vol. 100, no. 2–3, pp. 324-328, 2006. doi:10.1016/j.matchemphys.2006.01.010

[11] O. Bernard, A.M. Huntz, M. Andrieux, W. Seiler, V. Ji and S. Poissonnet, "Synthesis, structure, microstructure and mechanical characteristics of MOCVD deposited zirconia films," *Applied Surface Science*, vol. 253, no. 10, pp. 4626-4640, 2007. doi:10.1016/j.apsusc.2006.10.025

[12] M. Mishra, P. Kuppusami, A. Singh, S. Ramya, V. Sivasubramanian, E. Mohandas, "Phase evolution in zirconia thin films prepared by pulsed laser deposition," *Applied Surface Science*, vol. 258, no.12, pp. 5157–5165, 2012. doi:10.1016/j.apsusc.2012.01.160

[13] D.Q. Xiao, G. He, P. Jin, J. Gao, J.W. Zhang, X.F. Chen, C.Y. Zheng, M. Zhang and Z.Q. Sun, "Effects of boron incorporation on the structural, optical and electrical properties of sol-gel-derived ZrO2 gate dielectrics," *Journal of Alloys and Compounds*, vol. 649, pp. 1273-1279, 2015. doi:10.1016/j.jallcom.2015.07.210

[14] H.P. Jee, B.Y. Young, H.L. Keun, S.J. Woo, Y.O. Jin, S.C. Soo, W.L. Hyun, W.H. Sun and K.B. Hong, "Boron-doped peroxo-zirconium oxide dielectric for high-performance, low-temperature, solution-processed indium oxide thin-film transistor," ACS applied materials \& interfaces, vol.5, no. 16, pp.8067-8075, 2013. doi:10.1021/am402153g

[15] V. S. Anitha, S. S. Lekshmy and K. Joy, "Effect of annealing temperature on optical and electrical properties of ZrO2–SnO2 nanocomposite thin films," *Journal of Materials Science: Materials in Electronics*, vol. 24, pp. 4340–4345, 2013. doi:10.1007/s10854-013-1408-7

[16] A. Goktas, F. Aslan and İ.H. Mutlu, "Annealing effect on the characteristics of $La_{0.67}Sr_{0.33}MnO_3$ polycrystalline thin films produced by the sol–gel dip-coating process," *Journal of Materials Science: Materials in Electronics*, vol. 23, pp. 605–611, 2012. doi:10.1007/s10854-011-0448-0

[17] I. J. Berlin, S. S. Lekshmy, V. Ganesan, P.V. Thomas and K. Joy, "Effect of Mn doping on the structural and optical properties of ZrO_2 thin films prepared by sol–gel method," *Thin Solid Films*, vol. 550, pp. 199-205, 2014. doi:10.1016/j.tsf.2013.10.164

[18] A. Goktas, F. Aslan, A. Tumbul and S. Gunduz, "Tuning of structural, optical and dielectric constants by various transition metal doping in ZnO:TM (TM=Mn, Co, Fe) nanostructured thin films: A comparative study," *Ceramics International*, vol. 43, no. 1, pp. 704-713, 2017. doi:10.1016/j.ceramint.2016.09.217

[19] A. Goktas, I. H. Mutlu and Y. Yamada, "Influence of Fe-doping on the structural, optical, and magnetic properties of ZnO thin films prepared by sol–gel method," *Superlattices and Microstructures*, vol. 57, pp. 139-149, 2013. doi:10.1016/j.spmi.2013.02.010

[20] A. Méndez-López, O. Zelaya-Ángel, M. Toledano-Ayala, I. Torres-Pacheco, J. F. Pérez-Robles and Y. J. Acosta-Silva, "The Influence of Annealing Temperature on the Structural and Optical Properties of ZrO2 Thin Films and How Affects the Hydrophilicity," Crystals, vol. 10, no. 6, pp. 454. 2020. doi:10.3390/cryst10060454

[21] H. Gencer, A. Goktas, M. Gunes, H.I. Mutlu and S. Atalay, "Electrical Transport and Magnetoresistance Properties of La0.67Ca0.33MnO3 Film Coated On Pyrex Glass Substrate," *International Journal of Modern Physics B*, vol. 22, no. 05, pp. 497-506, 2008. doi:10.1142/S0217979208038776

[22] Y. Mansilla, M. D. Arce, C. González-Oliver, J. Basbus, H. Troiani and A. Serquis, "Characterization of stabilized ZrO_2 thin films obtained by sol-gel method," *Applied Surface Science*, vol. 569, pp. 150787, 2021. doi:10.1016/j.apsusc.2021.150787

[23] A. Göktaş, A. Tumbul, F. Aslan, "Grain size-induced structural, magnetic and magnetoresistance properties of $Nd_{0.67}Ca_{0.33}MnO_3$ nanocrystalline thin films," *Journal of Sol-Gel Science and Technology*, vol. 78, pp. 262–269, 2016. doi:10.1007/s10971-016-3960-0

[24] F. Mikailzade, F. Önal, M. Maksutoglu, M. Zarbali and A. Göktaş, "Structure and Magnetization of Polycrystalline $La_{0.66}Ca_{0.33}MnO_3$ and $La_{0.66}Ba_{0.33}MnO_3$ Films Prepared Using Sol-Gel Technique," *Journal of Superconductivity and Novel Magnetism*, vol. 31, pp. 4141–4145, 2018. doi:10.1007/s10948-018-4683-y

[25] M. Boulouz, L. Martin, A. Boulouz and A. Boyer, "Effect of the dopant content on the physical properties of Y_2O_3–ZrO2 and CaO–ZrO_2 thin films produced by evaporation and sputtering techniques," *Materials Science and Engineering: B*, vol. 67, no. 3, pp. 122-131, 1999. doi:10.1016/S0921-5107(99)00338-4

[26] W.T. Tang, Z.F. Ying, Z.G. Hu, W.W. Li, J. Sun, N. Xu and J.D. Wu, "Synthesis and characterization of HfO_2 and ZrO_2 thin films deposited by plasma assisted reactive pulsed laser deposition at low temperature," *Thin Solid Films*, vol. 518, no. 19, pp. 5442-5446, 2010. doi:10.1016/j.tsf.2010.04.012

[27] D. Tahir, E. Kyoung Lee, S. Kun Oh, H. Jae Kang, S. Heo, J. Gwan Chung, J. Cheol Lee and S. Tougaard, "Dielectric and optical properties of Zr silicate thin films grown on Si (100) by atomic layer deposition," *Journal of Applied Physics*, vol. 106, no. 8, pp. 084108-14, 2009. doi:10.1063/1.3246612

[28] A. Goktas, F. Aslan, B. Yeşilata and İ. Boz, "Physical properties of solution processable n-type Fe and Al co-doped ZnO nanostructured thin films: Role of Al doping levels and annealing," *Materials Science in Semiconductor Processing*, vol. 75, pp. 221-233, 2018. doi:10.1016/j.mssp.2017.11.033

[29] M. T. Soo, N. Prastomo, A. Matsuda, G. Kawamura, H. Muto, A. F. M. Noor, Z. Lockman and K. Y. Cheong, "Elaboration and characterization of sol–gel derived ZrO_2 thin films treated with hot water," *Applied Surface Science*, vol. 258, no. 13, pp. 5250-5258, 2012. doi:10.1016/j.apsusc.2012.02.008

[30] S. Chang and R. Doong, "The Effect of Chemical States of Dopants on the Microstructures and Band Gaps of Metal-Doped ZrO_2 Thin Films at Different Temperatures," *The Journal of Physical Chemistry B*, vol. 108, no. 46, pp. 18098-18103, 2004. doi:10.1021/jp047440n